ACS NANO

www.acsnano.org

ARTICLE

Random Metastructures for Nanoscale Visualization of Single-Exosome Dynamics in a Gut–Brain-Axis-on-a-Chip

Hongki Lee,[‖] Gwang Myeong Seo,[‖] Hajun Yoo, Gwiyeong Moon, Hyunwoong Lee, Zhaowei Liu, Jong Hwan Sung, and Donghyun Kim*

Cite This: *ACS Nano* 2025, 19, 30349–30360

Read Online

ACCESS | Metrics & More | Article Recommendations | Supporting Information

ABSTRACT: **This study introduces an innovative nanophotonic biosensor system designed to explore exosome dynamics within the gut–brain axis, highlighting the bidirectional and biochemical communication between the gastrointestinal tract and the central nervous system. The proposed system incorporates coculture environments for various cell types, microfluidic control of exosomes, and super-resolution imaging capabilities for both exosomes and live cells. While enabling real-time observation of long-range exosome dynamics within the gut–brain-axis-on-a-chip, this approach offers superior spatial resolution for visualizing individual exosomes in both donor and recipient cells. Through precise microfluidic manipulation, exosomes are observed as they are secreted from donor cells, transported within the chip, and interact with recipient cells in a coculture environment, mimicking the communication process occurring in the gut–brain axis. The dynamics of exosome transport within the gut–brain axis model are expected to improve the understanding of their biological functions and potential applications.**

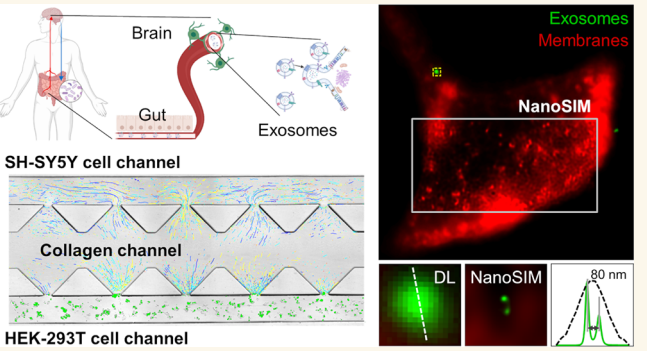

KEYWORDS: *super-resolution microscopy, metastructures, structured illumination microscopy, exosomes, gut–brain-axis-on-a-chip, microfluidic chip*

Exosomes are membrane-bound extracellular vesicles that are secreted by cells when multivesicular bodies fuse with the cell plasma membrane, releasing intraluminal vesicles in the extracellular space. Exosomes are known to perform the delivery of proteins and RNAs for cell-to-cell signaling, carry cell-specific markers, and participate in physiological and pathological processes.[1,2] Despite their clinical potential, much remains unknown about their physical properties and biological functions. Exosomes are notably smaller than the diffraction limit of light, posing challenges for imaging and analysis. Detailed nanoscale analysis of exosomes often relies on high-resolution techniques such as electron microscopy or atomic force microscopy (AFM). Optical observation of exosomes has been achieved using diffraction-limited methods like time-lapse fluorescence confocal microscopy and dark-field microscopy.[3−7] Due to their small size and limited scattering cross-section, exosomes often require specialized analytical methods, such as plasmonic imaging and detection[8,9] and interferometric scattering micrsocopy[10] where exosome size distribution can be analyzed through their scattering intensity. Super-resolution localization microscopy has also been employed to visualize exosomes,[11] but despite recent advancements, these techniques often suffer from poor spatiotemporal resolution, limiting the ability to capture dynamic processes.

Here, we present the nanoscale observation of exosome dynamics in an *in vitro* microfluidic coculture environment using nanospeckle illumination microscopy (NanoSIM). NanoSIM utilizes random metastructures to generate near-field speckles for super-resolved image reconstruction. The near-field speckles enhance resolution through azimuthal scanning illumination (ASI) by exciting localized surface plasmons (LSPs) on metastructures. Such a near-field speckle pattern is useful for achieving higher imaging resolution than traditional structured illumination microscopy (SIM). Unlike

Received: June 2, 2025
Revised: August 7, 2025
Accepted: August 8, 2025
Published: August 14, 2025

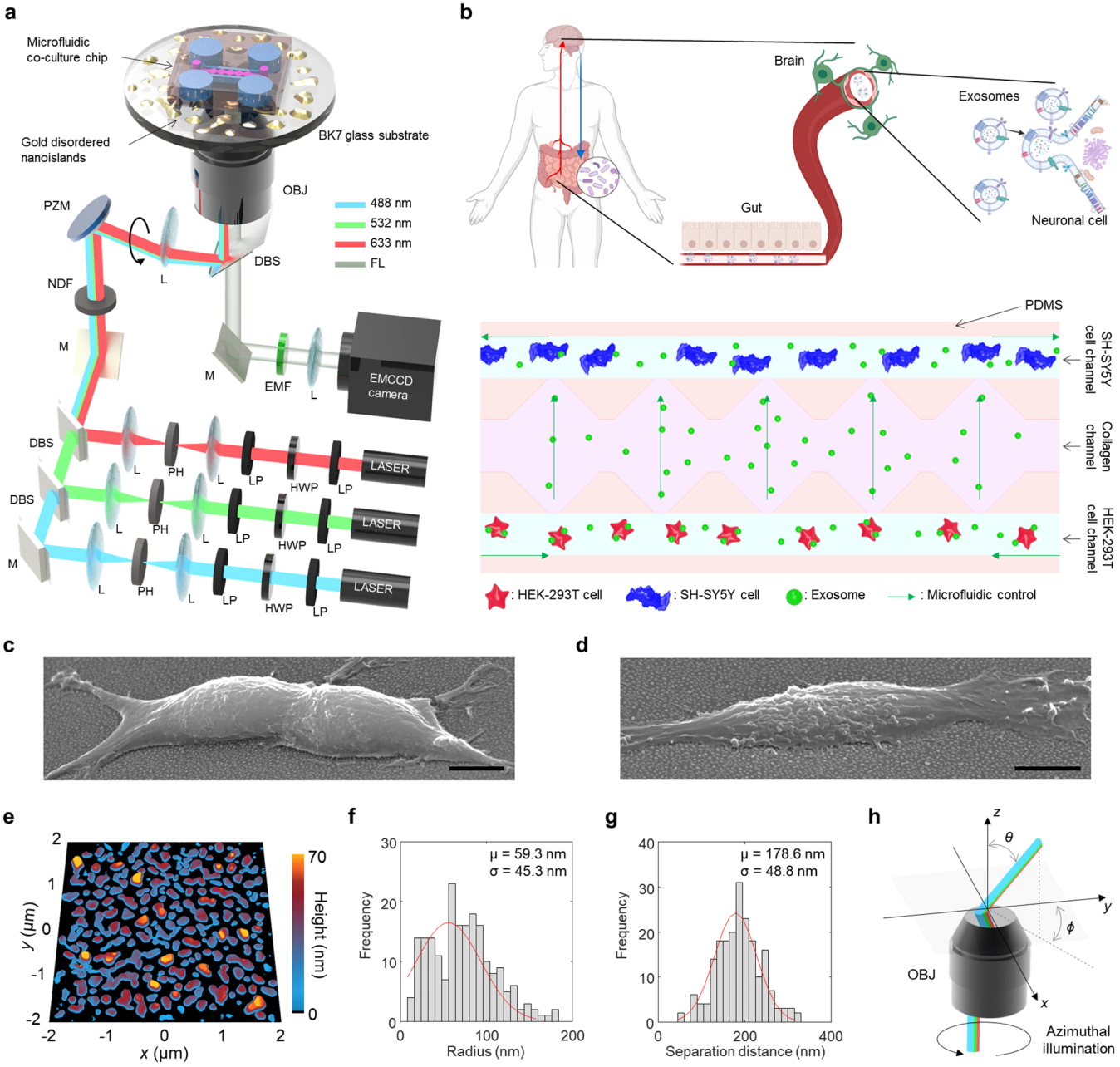

Figure 1. Schematics of nanospeckle illumination microscopy with a coculture microfluidic chip. (a) The optical setup with random metastructure substrates with a coculture microfluidic chip (LP: linear polarizer, HWP: half-wave plate, L: lens, PH: pinhole, M: mirror, DBS: dichroic beamsplitter, NDF: neutral density filter, PZM: piezoelectric mirror, OBJ: objective lens, EMF: emission filter). (b) Schematic of microfluidic GBA-on-a-chip for reproducing the extracellular vesicle exchange between the gut and brain cells. (c,d) SEM images of (c) human embryonic kidney (HEK-293T) cells and (d) human neuroblastoma (SH-SY5Y) cells on random metastructure substrate. Scale bar: 5 μm. (e) An AFM image of a random metastructure substrate consisting of gold nanoislands. (f,g) The morphological features of random metastructures: (f) radius and (g) separation distance to the nearest neighboring nanoislands. The histograms are fitted to a Gaussian distribution function. (h) Detailed description of azimuthal scanning illumination with different incident light sources.

traditional SIM, these patterns allow for the sampling and reconstruction of features much smaller than the diffraction limit. Image reconstruction is performed using algorithms that do not require prior knowledge of the exact illumination patterns. By combining multiple subframe images, the technique effectively achieves super-resolution. Notably, the random metastructures can be mass-produced over large sample areas via simple film deposition followed by thermal annealing. This approach has been widely explored in applications such as optical sensing,[12−15] Raman signal enhancement,[16−18] fluorescence microscopy,[19] and enhanced surface plasmon resonance (SPR) detection.[20−22]

We integrate NanoSIM with a gut−brain axis (GBA) organ-on-a-chip. The GBA represents biochemical communication networks between the gastrointestinal tract and the central nervous systems, encompassing the nervous and circulatory systems.[23] Microfluidic organ-on-a-chip platforms, designed to mimic human physiology, have proven valuable for studying various physiological and pathological aspects of human tissues and the complex interactions between various organs.[24] While

https://doi.org/10.1021/acsnano.5c09164
ACS Nano 2025, 19, 30349−30360

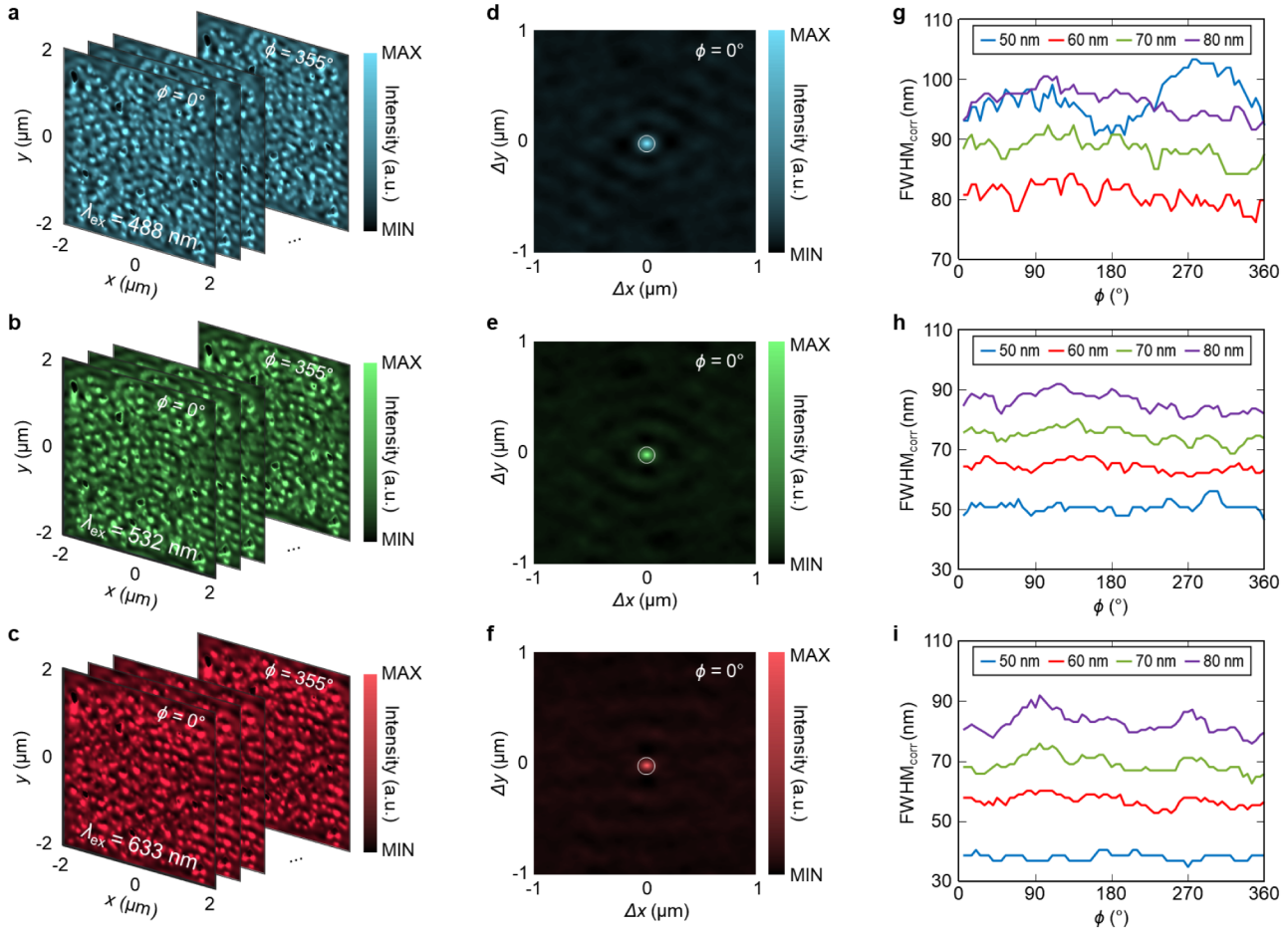

Figure 2. Switching near-fields with azimuthal scanning illumination on random metastructure substrate. (a−c) The numerical calculation of localized near-fields of plasmonic metastructure substrate based on the morphology information obtained by AFM at different incident wavelengths of λ_{ex} = (a) 488, (b) 532, and (c) 633 nm at the height of 50 nm. 72 near-field distributions with different azimuthal angles ϕ ranging from 5° to 360° in a step of 5° are obtained to confirm the total illumination coverage on the substrate's surface and the performance of spatial sampling. (d−f) The image autocorrelation of nanospeckle illuminations with different incident wavelengths of λ_{ex} = (d) 488, (e) 532, and (f) 633 nm at ϕ = 0°. (g−i) represent the full-width at half maximum ($FWHM_{corr}$) of the autocorrelation functions in (d−f) at different heights of h = 50−80 nm from the gold−glass interface (h = 0 nm), respectively.

previous studies have used organ-on-a-chip technology to replicate the GBA by coculturing intestinal cells and gut microbiota with neuronal cells, a common limitation is the inability to simultaneously coculture intestinal and brain neural cells, requiring a separate purification step for exosomes.[25,26] This limitation impedes the real-time observation of exosome secretion and delivery.

The integration of NanoSIM with the GBA-on-a-chip provides an innovative platform that enables the coculture of intestinal and neuronal cells, microfluidic manipulation of secreted exosomes, and super-resolution imaging of exosome transport. The chip consists of spatially separated but fluidically connected gut and brain cell chambers, allowing for exosome passage across both the epithelial and blood−brain barriers.[27] This system substantially improves our capacity to study exosome-mediated communication within the GBA and opens new avenues for exploring their roles in both physiological and pathological processes.[28,29]

RESULTS

Super-Resolution NanoSIM with GBA-on-a-Chip. Figure 1a represents our broadband super-resolution NanoSIM system to achieve nanoscale visualization of exosomes at donor and recipient cells within a microfluidic chip that mimics an *in vivo* microenvironment for the intercellular transport of exosomes. Donor and recipient cells are cultured in a GBA-on-a-chip, which is attached to the plasmonic disordered substrate. The complete workflow is detailed in Supplementary section 1. Here, the donor cells represent gastrointestinal cells and the recipient cells represent brain cells. Wide-field fluorescence images provide the dynamics of exosomes at plasma membranes and intracellular environments of donor and recipient cells, as well as microfluidic transport within the chip channels whose detailed dimensions are presented in Supplementary section 2. In this study, we use human embryonic kidney (HEK-293T) cells transfected with a plasmid to express fluorescently labeled exosomes. Supplementary section 3 demonstrates that the live cells can also be replaced with different types of cells, such as a gut cell line (Caco-2 cells). While culturing the gut cells as the donor cells would be physiologically more realistic, transfected HEK-293T cells offer better efficiency in producing fluorescently labeled exosomes. Therefore, in our GBA-on-a-chip, we employ HEK-293T cells as donor cells to represent gut-secreted exosomes.

As shown in Figure 1b, HEK-293T cells secrete exosomes into the microfluidic channel. Exosomes present in the donor

https://doi.org/10.1021/acsnano.5c09164
ACS Nano 2025, 19, 30349−30360

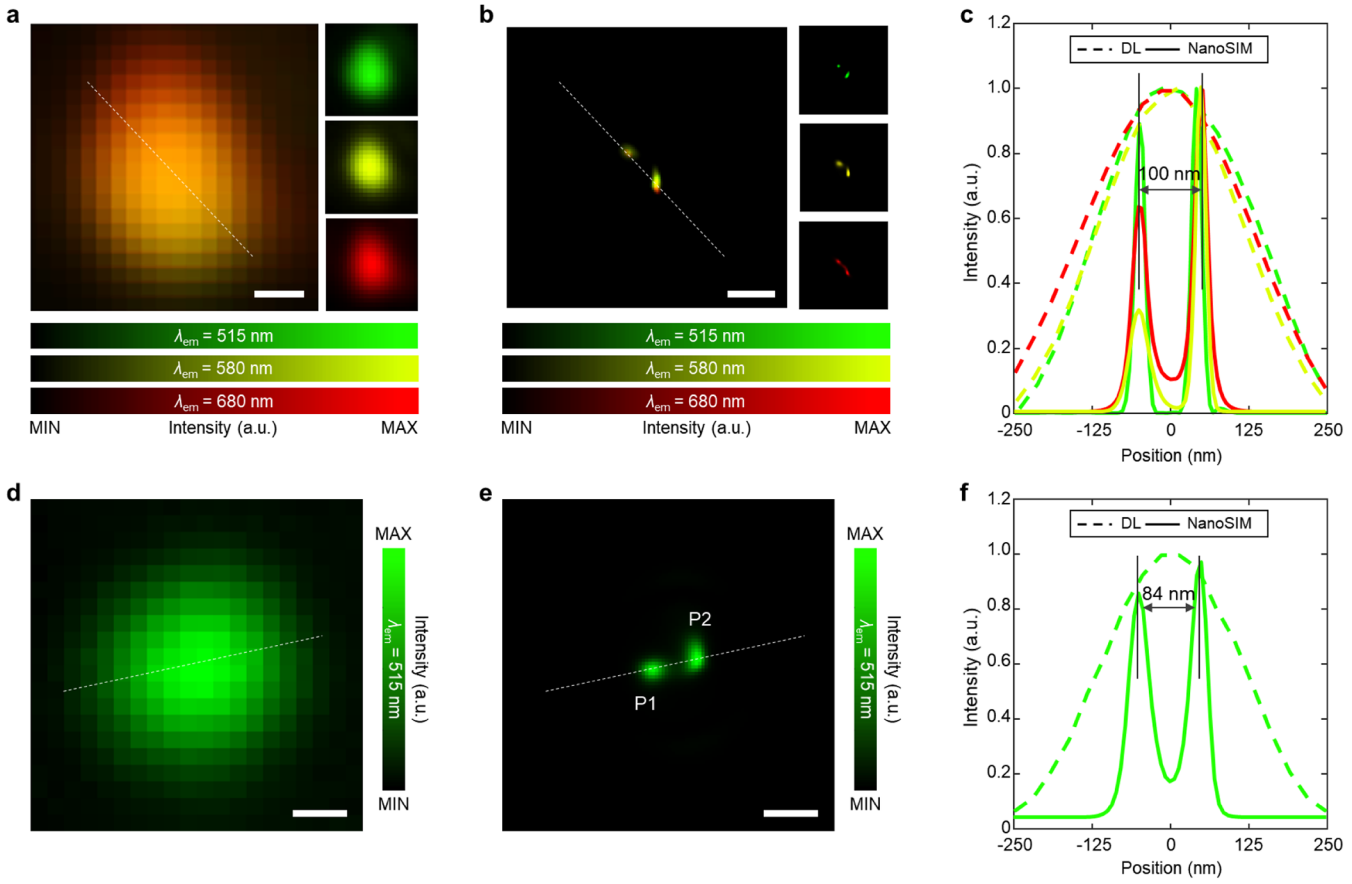

Figure 3. Broadband super-resolution imaging by NanoSIM. (a) Diffraction-limited fluorescence image of aggregated polystyrene nanobeads containing different fluorescence dyes on plasmonic metastructures. An image data set of 180 frames was obtained under ASI for each λ_{ex} = 488, 532, and 633 nm. The overlaid images of each data set with different fluorescence emissions at λ_{em} = 515, 580, and 680 nm are shown. (b) Super-resolution image reconstruction for fluorescence nanobead images at different emission wavelengths using NanoSIM. (c) Normalized intensity profiles along the white dashed lines in (a,b). (d) Diffraction-limited fluorescence image of aggregated exosomes on disordered plasmonic nanosubstrate. An image data set of 90 frames was obtained under ASI at λ_{ex} = 488 nm. (e) Super-resolution image reconstruction of aggregated exosomes using NanoSIM. (f) Normalized intensity profiles along the white dashed lines in (d,e). Scale bars: 100 nm.

cell channel can be transported to the recipient channel containing human neuroblastoma (SH-SY5Y) cells after crossing the collagen channel in the middle, which separates the donor and recipient channels. The convective flow in the GBA-on-a-chip is determined by controlling the amount of liquid in the reservoirs in the chip, whose detailed operation is discussed in the following sections. The scanning electron microscopy (SEM) images of HEK-293T cells and SH-SY5Y cells cultured on the random metastructure substrate are shown in Figure 1c,d, which indicate good cell viability. The random metastructure substrate is used for the super-resolution reconstruction of exosomes at plasma membranes and the intracellular environments of HEK-293T and SH-SY5Y cells. The surface morphology of the metastructure is shown in Figure 1e. The plasmonic random metastructure substrate consists of annealed gold nanoislands that have a smaller size with a radius of 59.3 ± 45.3 nm and a denser distribution with a separation distance of 178.6 ± 48.8 nm, compared to the previous study, as described in Figure 1f,g. Such subdiffraction-limited morphological features of randomly distributed gold nanoislands enable nanospeckle spatial sampling with LSP excitation for wide-field super-resolution image reconstruction.[16,19,30,31] Figure 1h represents the ASI with three incident wavelengths to conduct broadband nanospeckle illumination at biological targets labeled with different fluorescent dyes.

Multicolor LSP-Enhanced Imaging Resolution. The plasmonic disordered substrate exhibits a broadband optical response due to its random morphological characteristics. Here, nanospeckles refer to localized near-field distributions generated by random metastructures, in contrast to conventional far-field speckles. Such nanospeckles on the substrate surface can be excited at visible wavelengths of λ_{ex} = 488, 532, and 633 nm as presented in Figure 2a−c, which are obtained by using the finite-difference time-domain (FDTD) method with the morphological information on the disordered substrate shown in Figure 1d. The presence of localized near-field distributions and multiple scattered surface waves on the random metastructure is experimentally confirmed via near-field scanning optical microscopy.[32] An example of ASI with a step of ϕ = 5° ranging from 5 to 360° in Figure 2a−c shows that the total illumination can cover the nanosubstrate surface during ASI. ASI produces a large number of statistically distinct subframe images, each capturing different spatial frequency information from the sample. These subframes are then used for high-resolution image reconstruction. Figure 2d−f shows the image autocorrelation of nanospeckle illumination with different incident wavelengths of λ_{ex} = 488,

https://doi.org/10.1021/acsnano.5c09164
ACS Nano 2025, 19, 30349−30360

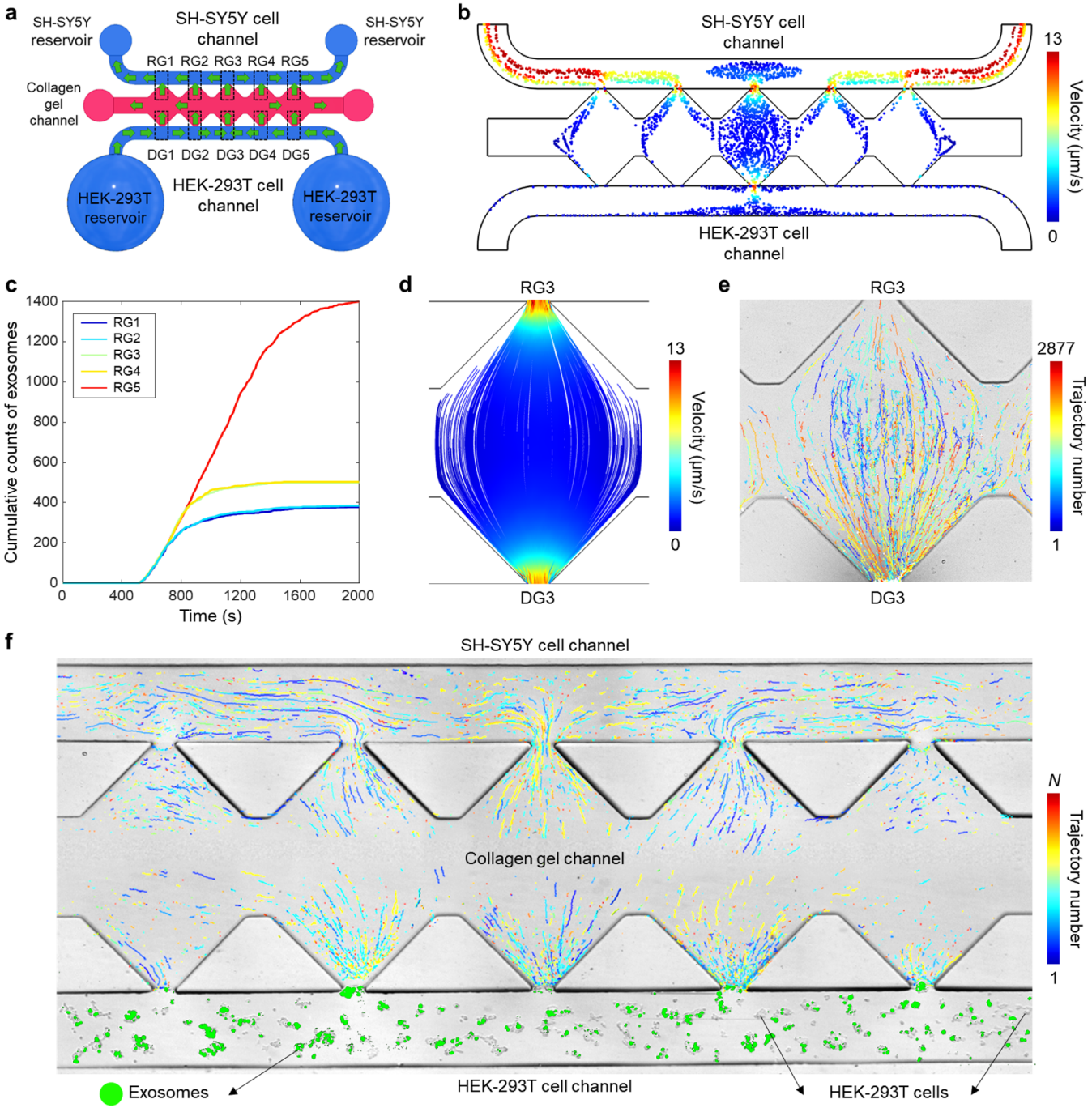

Figure 4. Microfluidic control of GBA-on-a-chip. (a) Top-view illustration of the microfluidic chip. The exosomes are secreted by HEK-293T cells and move to the SH-SY5Y channel through the donor gates (DGs), the collagen gel channel, and the receptor gates (RGs). The green arrows represent the direction of microfluidic control. (b) The distribution of exosomes in the chip is calculated by the numerical simulation at 800 s after release from the donor cells. (c) The cumulative counts of exosomes that passed through each RG from 0 to 2000 s. (d) The velocity distribution of exosomes being transported in the collagen channel between DG3 and RG3. The trajectory is obtained based on the simulated transport of exosomes from 0 to 1000 s. (e) Exosome tracking in the collagen channel between DG3 and RG3. (f) The total trajectories in each gate area are measured to be $N = N_{RG1 \sim 5}$ and $N_{DG1 \sim 5}$ (see details in Supplementary section 8).

532, and 633 nm when $\phi = 0°$. The autocorrelation functions indicate that the localized near-field distribution is random, with the peak at zero displacement ($\Delta x = 0$ and $\Delta y = 0$) and has a full width at half maximum (FWHM) that represents the sampling spatial frequency. The $FWHM_{corr}$ represents the higher spatial frequency of near-field distribution compared to the diffraction-limited far-field speckles generated by LSP. As shown in Figure 2g–i, the $FWHM_{corr}$ can be maintained as subdiffraction-limited during ASI. This near-field distribution induced by ASI implies that plasmonic disordered substrate can generate wide-field subframe images of fluorescence-labeled molecules for SIM. The spatial sampling frequency of a fluorescence image is directly influenced by the subdiffraction-limited size of nanospeckles formed at random metastructures with a radius of 59.3 ± 45.3 nm and a separation distance of 178.6 ± 48.8 nm, which is more suitable than the previous

https://doi.org/10.1021/acsnano.5c09164
ACS Nano 2025, 19, 30349−30360

work.[19] In Figure 2g–i, the $FWHM_{corr}$ tends to decrease at longer wavelengths, where conventional fluorescence image resolution can be improved by high spatial sampling. In this study, near-field excitation on random metastructures at the wavelength of 488 nm is chosen for the super-resolution imaging of exosomes tagged with green fluorescent protein (GFP).[33,34]

NanoSIM Imaging of Aggregated Nanobeads and Exosomes. Figure 3 demonstrates the broadband super-resolution image reconstruction of various single nanoparticles by NanoSIM. Figure 3a–c compares a raw image of fluorescent polystyrene (PS) nanobeads (radius = 49.5 ± 4 nm) with a super-resolution image reconstructed by NanoSIM. Fluorescence images of multicolor PS beads stained with different fluorescent dyes are acquired with incident laser beams at 488, 532, and 633 nm. Based on the near-field speckles generated by ASI from ϕ = 2 to 360° in a step of 2°, 180 frames of fluorescence images (pixel size = 30 × 30 nm^2) are used to generate a super-resolved nanobead image (pixel size = 5 × 5 nm^2) with the blind-SIM algorithm.[35] As shown in Figure 3b,c, NanoSIM can improve the image resolution of two aggregated nanobeads in the raw image. The separation distance of two beads is observed to be 95, 100, and 100 nm acquired at the emission peaks of 515, 580, and 680 nm, respectively. The correlation study between super-resolution reconstruction image by NanoSIM and AFM image was conducted in the previous work.[19] Here, the deviation in the positions of two particles at different emission wavelengths is due to molecular localization shifts caused by plasmonic coupling. Since many fluorescent molecules can exist inside a nanoparticle with mixed dipole orientations, mislocalization induced by plasmon–molecule coupling is averaged and becomes less effective.[36] Figure 3d–f represents the super-resolution image reconstruction of the aggregated exosomes. After conducting NanoSIM image reconstruction, we identified at least two different exosomes present at separate positions, as described in Figure 3e. At the positions of P1 and P2, two individual exosomes are resolved with a separation distance of 84 nm. NanoSIM can achieve image resolution below 100 nm as confirmed by autocorrelation functions of nanospeckle distributions in the previous section. The reconstructed images of individual exosomes have good agreement with the size and shape distribution of exosomes[37,38] (more examples are demonstrated in Supplementary section 4).

Microfluidic Control for Exosome Transport in GBA-on-a-Chip. To model exosome transport from the gut epithelium to brain tissue *in vitro*, we implemented convective flow in our GBA-on-a-chip by utilizing surface tension–driven pressure differences between the chip's reservoirs. This design choice was guided by physiological observations that exosomes reach the brain within 5 min following intravenous injection in mice.[39] Considering the slower systemic circulation in humans and comparable interstitial flow velocities across species, we estimated a gut-to-brain transit time of approximately 6–8 min.[40,41] Achieving this time scale across the 1.3-mm collagen gel barrier in our chip requires an interstitial velocity of 2–3 μm/s, which can be generated by passive convection. In contrast, diffusive transport is not only significantly slower but also inconsistent with *in vivo* physiology, where flow-mediated delivery predominates. For instance, a 200-nm exosome diffusing in 2 mg/mL collagen (diffusion coefficient ~ 1 × 10^{-12} m^2/s) would take over 130 h to traverse just 1 mm. Chemical gradient–based approaches are likewise unsuitable, as they require continuous infusion of purified exosomes and fail to capture endogenous secretion from live epithelial cells. Therefore, we employed convection as the primary transport mechanism to mimic physiologically relevant delivery and to enable real-time tracking from epithelial secretion to neuronal interaction (see details in Supplementary section 5).

The GBA-on-a-chip was designed to model the directional transport of epithelial exosomes from the gut to the brain, recapitulating their physical passage from the intestinal barrier to neuronal cells. To enable high-resolution, real-time single-exosome imaging, we required a donor epithelium capable of producing exosomes with stable fluorescent labeling. Intestinal cell lines such as Caco-2 are widely used in gut models but exhibited an extremely low transfection efficiency, resulting in insufficient fluorescence for reliable tracking. HEK-293T cells, by comparison, offer a high transfection efficiency and are frequently used in brain-related exosome studies. Exosomes derived from HEK-293T cells interact with SH-SY5Y cells, a human neuronal cell line, and have been applied in neurodegenerative disease models such as Parkinson's and Alzheimer's diseases.[42,43] Moreover, exosome biogenesis is governed by a conserved set of proteins across epithelial lineages, including Endosomal Sorting Complex Required for Transport (ESCRT), which is a protein machinery responsible for exosome biogenesis, with components such as TSG101 and ALIX, generating vesicles with a common membrane protein family known as tetraspanins, such as CD63, CD81, and CD9;[44] organ-specific differences in this process have not been clearly demonstrated. We further confirmed that Caco-2 and SH-SY5Y cells remained viable in coculture and that exosomes from either source would follow comparable trajectories under the convection-driven flow conditions in the device. Based on these considerations, we used HEK-293T cells transfected with CD63–GFP as a surrogate for the intestinal epithelium in this transport-focused model.

In the HEK-293T cell channel, there are five exits through which exosomes are released into the collagen gel channel, named donor gates (DG1–5). In the SH-SY5Y cell channel, there are also five entrances for exosomes entering from the collagen gel channel, labeled as receptor gates (RG1–5). Using numerical simulation, we explore the time-lapse process of transferring exosomes from the HEK-293T cell channel to the SH-SY5Y cell channel via the formation of a convective flow. The parameters used in the simulation model are summarized in Supplementary section 6. As shown in Figure 4b and Supplementary section 7, we confirm that exosomes in the HEK-293T cell channel mainly converge at DG3 due to the internal convective flow formed within the channel. Exosomes that have crossed the collagen gel channel move in both directions toward the SH-SY5Y channel reservoirs. Based on the observed flow patterns within the microfluidic chip, exosomes originating from the HEK-293T cell channel are anticipated to converge toward DG3, significantly enhancing their likelihood of reaching RG3 compared to other RGs. Figure 4c shows the cumulative counts of exosomes released from the HEK-293T channel, reaching each RGs within the period of 0 to 2000 s. Additionally, we analyze the trajectory of exosome movements from DG3 to RG3 as shown in Figure 4c,d. We observe that after 1000 s, most of the new exosomes reach RG3. The number of exosomes reaching RG3 continues to increase until 2000 s.

From the experimental examination of the exosome trajectories moving from DG3 to RG3 as shown in Figure

https://doi.org/10.1021/acsnano.5c09164
ACS Nano 2025, 19, 30349–30360

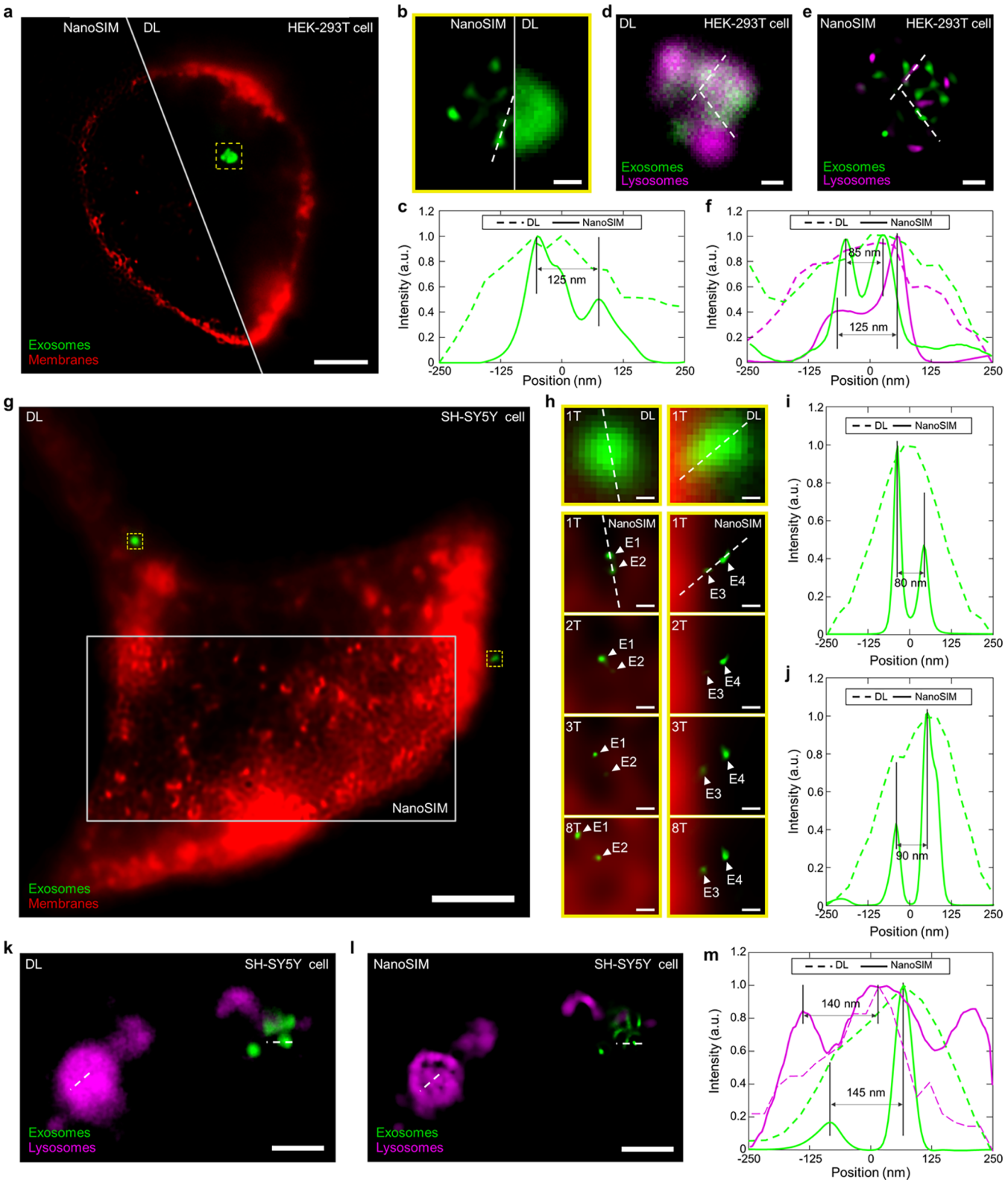

Figure 5. Super-resolution images of exosomes, plasma membranes, and lysosomes within a coculture environment representing the dynamic behavior of exosomes. (a) Diffraction-limited (DL) fluorescence image of exosomes (green) and plasma membrane (red) in a live HEK-293T cell. Plasma membranes are conjugated with Alexa Fluor 633. (b) Super-resolution image reconstructions for CD63-GFP exosomes. (c) Normalized intensity profiles along the white dashed lines in (b). (d) Diffraction-limited fluorescence image of exosomes (green) and lysosomes (magenta) inside a live HEK-293T cell. (e) Super-resolution image reconstructions for CD63-GFP exosomes and LysoTracker-Deep-Red lysosomes. (f) Normalized intensity profiles along the white dashed lines in (d,e). (g) Diffraction-limited fluorescence image of exosomes (green) and plasma membrane (red) in a live SH-SY5Y cell. (h) Super-resolution image reconstructions for CD63-GFP exosomes and plasma membranes conjugated with Alexa Fluor 633. *T* denotes the time-lapse period of 3.6 s. (i) Normalized intensity profiles along the white dashed lines in the left column of (h). (j) Normalized intensity profiles along the white dashed lines in the right column of (h). (k)

https://doi.org/10.1021/acsnano.5c09164
ACS Nano 2025, 19, 30349−30360

Figure 5. continued

Diffraction-limited fluorescence image of exosomes (green) and lysosomes (magenta) inside a live SH-SY5Y cell. (l) Super-resolution image reconstructions for CD63-GFP exosomes and LysoTracker-Deep-Red lysosomes. (m) Normalized intensity profiles along the white dashed lines in (j,k). Scale bars in (a,g), (b,d,e), (h), and (k,l) are 3 μm, 200 nm, 100 nm, and 1 μm, respectively.

4e, it is evident that exosomes released from DG3 migrated easily to RG3. The observed trajectories of CD63-GFP exosomes in the experiment described in Figure 4e showed a high correlation with the trajectories confirmed by the numerical simulation in Figure 4d, demonstrating successful exosome transport. Furthermore, we tracked CD63-GFP exosomes at all DGs and RGs in the GBA-on-a-chip with the convective flow, as shown in Figure 4f (see details in Supplementary section 8).

Super-Resolution Imaging of Exosomes, HEK-293T Cells, and SH-SY5Y Cells in GBA-on-a-Chip. Figure 5 illustrates the super-resolution imaging of live HEK-293T cells and SH-SY5Y cells in our GBA-on-a-chip, employing NanoSIM imaging to reveal previously unseen details of exosome transport. Live HEK-293T cells, transfected with GFP-tagged exosomes, are readily observed in the lower channel, as shown in Figure 4. We verify the presence of GFP-tagged exosomes within the cells and observe convection currents within the microfluidic environment, as shown in Figure 5a–f using an EM-CCD camera. In addition, cell membranes and lysosomes in HEK-293T cells are observed with a second EM-CCD camera. Intracellular exosomes exhibited a tendency to aggregate.[27] Before being released into the extracellular space, exosomes are intraluminal vesicles (ILVs) housed within multivesicular bodies (MVBs), with each MVB potentially containing multiple ILVs.[45] Figure 5b shows that individual exosomes are distinguishable only through the superior resolution of the NanoSIM. Figure 5c compares the intensity profiles in diffraction-limited and NanoSIM images, proving super-resolution imaging capabilities. As shown in Figure 5d,e, it is observed that exosomes and lysosomes overlap spatially in the HEK-293T cells. MVBs that do not fuse with the cell membrane to release ILVs externally can be degraded by lysosomes within the cell. Figure 5e provides significantly improved super-resolution, two-color images of exosomes and lysosomes.

After being transversed through the DG, collagen gel, and RG sequentially, exosomes reach the SH-SY5Y cell membranes. As expected from previous studies, their diffusion dynamics near these SH-SY5Y receptor cells exhibit distinct characteristics, depending on exosome–cell interactions.[46] In contrast to the convection-driven flow observed in other regions, exosomes exhibit confined movements near these neuronal cell membranes (see details in Supplementary section 9). Specifically, in Figure 5g, the movement of exosomes is significantly more confined, showing the behavior of membrane-associated particles. We observe that aggregated exosomes move along with the directional extension of the SH-SY5Y cell dendrite (Supplementary movie 1). The super-resolution capabilities of NanoSIM are essential in resolving these aggregates into distinct individual exosomes, as demonstrated in Figure 5h–j. The distance between two exosomes (E1 and E2) shown in the left column of Figure 5h increases progressively (Supplementary movie 2). In the right column of Figure 5h, while the soma remains stationary, the confined exosomes (E3 and E4) show comparatively limited translocation (Supplementary movie 3). In Supplementary section 9, exosomes exhibit free and loosely confined diffusion with a typical velocity of 1–1.5 μm/s. In contrast, E1 exhibited an average translation velocity of 7 nm/s while bound to the cell membrane. This observation demonstrates the direct exosome uptake process, in which exosomes bind to cell surface receptors for signal transduction during intercellular communication. The stationary exosomes observed near the plasma membrane of SH-SY5Y cells are likely tethered through receptor-mediated interactions. Similar tethered exosomes are repeatedly observed in other SH-SY5Y cells and bEnd.3 cells (Supplementary sections 10 and 11). Furthermore, NanoSIM enabled clear differentiation between aggregated exosomes and lysosomes that are colocalized within SH-SY5Y cells, as illustrated in Figure 5k–m. This observation reveals both the receptor-mediated signaling pathway followed by exosomes and their internalization via the lysosomal pathway for degradation.

DISCUSSION

Our approach combines large-scale, mass-produced plasmonic metastructures with a microfluidic chip designed to mimic gut–brain biochemical interactions, enabling the capture of dynamic exosome behavior over extensive distances. This setup employs a conventional total internal reflection configuration for super-resolution fluorescence imaging within the microfluidic chip, allowing wide-field imaging and convenient assessment of regions of interest. The plasmonic random metastructures fabricated on the glass substrate generate subdiffraction-limited nanoscale illumination, particularly beneficial for microfluidic chips integrated into glass substrates.

In our experimental configuration, we observe numerous exosomes released from HEK-293T cells migrating toward SH-SY5Y cells, enabling investigation into exosome dynamics and intercellular communication. Here, the super-resolution imaging capability can prove valuable in elucidating individual exosome behavior with significant implications for understanding their interactions with diverse cell types and potential roles in various biological processes. For example, exosomes are involved in the GBA, facilitating communication between the gastrointestinal system and the brain. Exosomes derived from gut cells (Caco-2) treated with gamma-aminobutyric acid (GABA) can activate neuronal cells, suggesting that GABA may enhance neuronal activity and offer a potential therapeutic approach for AD.[47] In AD, exosomes can transmit pathogenic proteins like tau and amyloid beta (Aβ), contributing to the spread of AD-related pathology.[48−51] Our system enables high-resolution tracking of these exosomes, offering a way to map individual exosome trafficking patterns and correlate them with the spatial progression of AD pathology.[52]

Our findings show that not all exosomes traverse the RGs to reach their intended targets. This delivery efficiency can potentially be optimized through modifications to the microfluidic chip dimensions and control parameters. Optimization of barrier structures and adjustments in channel dimensions, such as reducing the width of the collagen channel, may be necessary for improved exosome reception. Faster super-resolution dynamics can be achieved with a

https://doi.org/10.1021/acsnano.5c09164
ACS Nano 2025, 19, 30349−30360

reduced number of subframe images and optimized reconstruction algorithms.[53,54] In summary, by enabling the direct observation of exosome dynamics at super-resolution in different cell types within a controlled environment, our research paves new avenues for understanding the exosome function and their involvement in more complex biological processes.

CONCLUSIONS

In this study, we developed an integrated platform that combines NanoSIM with a GBA organ-on-a-chip to achieve real-time, super-resolution visualization of exosome transport across physiologically relevant cellular barriers. By using plasmonic random metastructures for near-field speckle generation, NanoSIM enables wide-field, subdiffraction-limited imaging of exosomes with high spatial resolution. This capability, when coupled with a microfluidic coculture system, allows direct tracking of exosome secretion, transit, and uptake between intestinal epithelial and neuronal cells. Our approach captures both the dynamic movement and confined interactions of exosomes with target cells, revealing distinct modes of intercellular communication such as receptor-mediated signaling and lysosomal degradation. Importantly, this platform overcomes limitations of existing organ-on-a-chip models by supporting continuous coculture and eliminating the need for exosome isolation, thereby preserving physiological context. Beyond fundamental insights into exosome biology, the system offers a versatile framework for investigating the role of extracellular vesicles in neurological disorders, including Alzheimer's disease, and holds potential for evaluating therapeutic strategies targeting exosome-mediated pathways. Future efforts will focus on enhancing imaging speed, refining chip architecture, and expanding the approach to disease-relevant cell models. Overall, this work provides a powerful and scalable methodology to probe exosome dynamics in complex biological systems with nanoscale precision.

METHODS

Experimental Setup. NanoSIM utilizes a total internal reflection fluorescence microscopy (TIRFM) setup with adjustable light incidence, as depicted in Figure 1a. The system combines illumination from three lasers: an Ar-ion laser (λ = 488 nm, Melles Griot, USA), a solid-state continuous-wave laser (λ = 532 nm, Novota Photonics, USA), and a Helium−Neon laser (λ = 633 nm, Melles Griot, USA). Before reaching a sample, light passes through neutral density filters and a beam expander for collimation. While NanoSIM does not require specific polarization control, *p*-polarization can be maintained during azimuthal scanning by using a combination of polarizers and waveplates. Localized near-field illumination is spatially switched by a mounted mirror on a piezoelectric tip/tilt platform (Model No: E-517.I3, Physik Instrumente GmbH & Co. KG, Germany). Incident light is illuminated onto the sample through an objective lens (CFI Apo TIRF 100×, NA 1.49, Nikon, Japan). Two EM-CCD cameras (iXon Ultra 897 and iXon Ultra 888, Andor Technology, United Kingdom) are used for image acquisition with a frame rate of 25 fps. Specific emission filters are employed depending on the detected fluorescent signal: AT535/40m (Chroma, Bellows Falls, USA) for GFP emission, AT690/50m (Chroma, USA) for Alexa Fluor 633 and LysoTracker Deep Red, and ET542/LP (Chroma, USA) for emission at 580 nm. A multibandpass dichroic beam splitter (ZT488/532/633/830/1064rpc, Chroma, USA) separates the excitation and emission light paths.

Fabrication of Random Metastructure Substrate and Coculture Chip. Random metastructure is fabricated on a BK7 glass substrate and cleaned using sonication with acetone, isopropyl alcohol, and deionized water. A 15-nm-thick gold film is deposited onto the cleaned substrate via thermal evaporation. The gold-coated substrate is annealed at a high temperature (350 °C) on a hot plate, inducing dewetting of the gold film and forming nanoislands. Previous studies have demonstrated that the size distribution and interisland spacing of these nanoislands follow a normal distribution and are influenced by specific fabrication parameters.[19,32] To enhance adhesion between the PDMS chip and the substrate, gold nanoislands are selectively removed from the bonding area before the microfluidic chip assembly. The nanoislands are retained in the area of cell culture channels to facilitate super-resolution imaging of exosomes, HEK-293T cells, and SH-SY5Y cells. To ensure chip integrity for accurate measurements, microscopic observation of the behavior of GFP-labeled exosomes was performed before each experiment, confirming the absence of leaks.

Image Acquisition and Reconstruction. TetraSpeck Microspheres (100 nm, T7279, Invitrogen, USA) were used for the control experiment. NanoSIM relies on SIM, a technique that extends resolvable information beyond the diffraction limit of conventional optical systems, thereby enhancing the image resolution. In SIM, the image is reconstructed from a weighted sum of modulated images captured under different illumination angles in the *k*-space. Our approach employs a blind-SIM algorithm and varies the light incidence azimuthally to obtain the necessary subframe images. In NanoSIM, ASI offers advantages due to the use of random metastructures as localized illumination sources. For control experiments using polystyrene beads, 180 frames are obtained for super-resolution NanoSIM reconstruction. For live cell and exosome imaging, 90 frames are obtained. The 8-frame time-lapse for super-resolution exosome dynamics is generated with image acquisitions of 720 frames. More details on image reconstruction can be found elsewhere.[19]

Numerical Simulation. We conduct a three-dimensional FDTD simulation to analyze the near-field distribution generated by a random metastructure substrate. The excitation wavelengths for the localized near-fields are λ_{ex} = 488, 532, and 633 nm. The refractive index of gold is sourced from Palik.[55] The simulation space spans 2 × 2 μm^2 in the horizontal axes and 600 nm in the axial direction. The mesh size near the metastructure is set to 7.5 × 7.5 × 7.5 nm^3, with nonuniform mesh construction. The morphology of the metastructure is determined using AFM measurements.

We used COMSOL Multiphysics software to model the exosome transport driven by convective flow in the GBA chip. The convective flow, driven by a pressure gradient from the HEK-293T to SH-SY5Y channel, is simulated using the laminar flow module. The collagen gel channel, acting as a porous membrane, is represented within the module, integrating the Darcy permeability and collagen gel porosity parameters. Exosome transport is simulated with the particle tracing module utilizing values from the laminar flow module. We simulate the dynamics of exosome transport, which initiates from the HEK-293T cell channel over a time span

https://doi.org/10.1021/acsnano.5c09164
ACS Nano 2025, 19, 30349−30360

of 0 to 2000 s. Supplementary section 6 details the parameters used in the simulation.

Cell Coculture in GBA-on-a-Chip. In GBA-on-a-chip experiments, we use human embryonic kidney cells (HEK-293T, CRL-3216, ATCC, USA) as donor cells responsible for secreting fluorescent exosomes. HEK-293T cells are transfected with a plasmid containing the sequence for fluorescently labeled CD63-GFP protein, which is a tetraspanin protein found on exosome surfaces.[56] We use HEK-293T cells, which have a high transfection efficiency and are commonly used in exosome-based research for neurodegenerative diseases.[57] For example, Jurgielewicz et al. confirmed the uptake of fluorescently labeled exosomes secreted by transfected HEK-293T cells by SH-SY5Y cells.[58] Although HEK-293T cells are not gut-originated, Caco-2 and HEK-293T are both human-originated cells and, therefore, presumably share common exosome-releasing mechanisms. Our research is focused on real-time visualization of transport routes and kinetics of exosomes across different organs. Considering this limitation and experimental objectives, we speculate that HEK-293T cells can be a suitable alternative to Caco-2 cells.

On the other hand, human neuroblastoma cells (SH-SY5Y, 22266, Korean Cell Line Bank , Korea) served as the recipient cells to take up these fluorescent exosomes. All cells are cultured in Dulbecco's Modified Eagle Medium (11995-040, Gibco, USA) supplemented with 10% fetal bovine serum (Welgene, S001-01, Korea) and 1% penicillin−streptomycin (P4333, Sigma-Aldrich, USA) at 37 °C in a 5% CO_2 incubator. The culture media were changed every 2−3 days.

Before coculturing HEK-293T and SH-SY5Y cells on the GBA-on-a-chip, a collagen gel with a concentration of 2.0 mg/mL is introduced into the collagen gel channel. To prepare 100 μL of collagen at 2.0 mg/mL concentration, the following components are mixed: 1.58 μL of 1N NaOH (S1996, SAMCHUN CHEMICALS, Korea), 10 μL of 10× Dulbecco's phosphate-buffered saline (D5652, Sigma-Aldrich, USA), 19.8 μL of distilled water, and 68 μL of collagen, rat tail type 1 (354236, Corning, USA). The GBA-on-a-chip, filled with 2.0 mg/mL collagen gel in the collagen gel channel, is incubated for 30 min at 37 °C with 5% CO_2. Once the collagen gel has gelled, 20 μL of SH-SY5Y cells at a concentration of 7×10^6 cells/mL is introduced into the SH-SY5Y cell channel. These cells are then cultured for 24 h at 37 °C with 5% CO_2. After 24 h of culturing SH-SY5Y cells on the GBA-on-a-chip, 60 μL of transfected HEK-293T cells at a concentration of 7×10^6 cells/mL is introduced into the HEK-293T channel of the device. Subsequently, both transfected HEK-293T and SH-SY5Y cells are cocultured on the GBA-on-a-chip for an additional 24 h at 37 °C with 5% CO_2.

Transfection of HEK-293T. HEK-293T cells were transfected to generate cells that spontaneously release GFP-exosomes. HEK-293T cells were seeded in a 6-well plate (Corning, USA) at a concentration of 2.5×10^5 cells per well and cultured for 24 h at 37 °C with 5% CO_2. After 24 h, a diluted DNA total solution was prepared by combining 2.5 μg of pCT-CD63-GFP plasmid (CYTO120-PA-1, System Biosciences, USA) and 5 μL of Lipofectamine 3000 (L3000001, Invitrogen, USA) with 125 μL of Opti-MEM (31985-062, Gibco, USA). A diluted lipofectamine 3000 solution was created by mixing 5 μL of Lipofectamine 3000 with 125 μL of Opti-MEM. The diluted Lipofectamine 3000 solution and the diluted DNA total solution were combined in equal parts (1:1) and incubated at room temperature for 5 min. Subsequently, 250 μL of the combined solution was added to a 6-well plate containing cultured HEK-293T cells, followed by overnight incubation at 37 °C with 5% CO_2.

Fluorescence Staining of Cell Membrane and Lysosomes. To stain the membranes of transfected HEK-293T and SH-SY5Y cells in the GBA-on-a-chip, the culture medium in both the HEK-293T and SH-SY5Y cell channels is removed. Subsequently, two washes are performed using Hank's Balanced Salt Solution (HBSS, Sigma, USA). Next, 50 μL of wheat germ agglutinin Alexa Fluor 633 conjugate (WGA-633, Invitrogen, USA) is added at a concentration of 45 μg/mL, with 60 μL added to the HEK-293T cell channel and 20 μL added to the SH-SY5Y cell channel. This is followed by a 10-min incubation at 37 °C with 5% CO_2. After the incubation, the WGA-633 solution in both channels is removed, and the cells are washed twice with HBSS. Medium is then added to both channels.

To observe lysosomes in transfected HEK-293T and SH-SY5Y cells, LysoTracker Deep Red (L12492, Invitrogen, USA) is diluted in HBSS to a concentration of 50 nM. The culture medium in both the HEK-293T and SH-SY5Y cell channels is removed, and the cells are washed with HBSS. LysoTracker at a concentration of 50 nM is introduced with 60 and 20 μL for the HEK-293T and SH-SY5Y cell channels, respectively. The cells are then incubated for 1 h at 37 °C in 5% CO_2. After the incubation, the LysoTracker solution is removed from both cell channels. Subsequently, both channels are washed twice with HBSS, and fresh medium is added.

ASSOCIATED CONTENT

Supporting Information

The Supporting Information is available free of charge at https://pubs.acs.org/doi/10.1021/acsnano.5c09164.

Fabrication and design of a microfluidic chip integrated with plasmonic metastructure (Figures S1 and S2); coculture of Caco-2 and SH-SY5Y cells with live−dead viability assay (Figure S3); super-resolution NanoSIM imaging of nanobeads (Figure S4); convection flow generation in the GBA-on-a-chip (Figure S5); numerical simulation of exosome transport in a microfluidic chip (Figure S6); diffusion dynamics of exosomes near SH-SY5Y cells (Figure S7); tethered exosomes at SH-SY5Y cells under coculture conditions (Figure S8); tethered exosomes at bEnd.3 cells under coculture conditions (Figure S9); parameters for numerical microfluidic simulation and exosome trajectory counts at gate regions (Tables S1 and S2) (PDF)

AUTHOR INFORMATION

Corresponding Author

Donghyun Kim − *School of Electrical and Electronic Engineering, Yonsei University, Seoul 03722, Korea;* orcid.org/0000-0003-1960-0527; Email: kimd@yonsei.ac.kr

Authors

Hongki Lee − *School of Electrical and Electronic Engineering, Yonsei University, Seoul 03722, Korea;* Present Address: Department of Electrical and Computer Engineering, University of California, San Diego, CA 92093, United States; orcid.org/0000-0002-0655-1925

https://doi.org/10.1021/acsnano.5c09164
ACS Nano 2025, 19, 30349−30360

Gwang Myeong Seo − *Department of Chemical Engineering, Hongik University, Seoul 04066, Korea;* Present Address: School of Mechanical Engineering, Sungkyunkwan University, Suwon, Republic of Korea 16419
Hajun Yoo − *School of Electrical and Electronic Engineering, Yonsei University, Seoul 03722, Korea*
Gwiyeong Moon − *School of Electrical and Electronic Engineering, Yonsei University, Seoul 03722, Korea;* Present Address: LG Innotek, Magok R&D Campus, Seoul, Republic of Korea 07796
Hyunwoong Lee − *School of Electrical and Electronic Engineering, Yonsei University, Seoul 03722, Korea;* Present Address: ASML Korea, Hwasung, Gyeonggi-do, Republic of Korea 18449; orcid.org/0000-0003-1647-1301
Zhaowei Liu − *Department of Electrical and Computer Engineering, University of California, San Diego, California 92093, United States;* orcid.org/0000-0002-5732-8109
Jong Hwan Sung − *Department of Chemical Engineering, Hongik University, Seoul 04066, Korea;* orcid.org/0000-0002-4019-866X

Complete contact information is available at: https://pubs.acs.org/10.1021/acsnano.5c09164

Author Contributions

[‖]H.L. and G.M.S. contributed equally to this work. The data that support the findings of this study are available from the corresponding author upon reasonable request.

Notes

The authors declare no competing financial interest.

ACKNOWLEDGMENTS

This work was supported by the National Research Foundation of Korea (NRF) grant funded by the Ministry of Science and ICT of the Korean government (2022R1A4A2000748, RS-2024-NR121319, and RS-2025-00515495).

REFERENCES

(1) Valadi, H.; Ekström, K.; Bossios, A.; Sjöstrand, M.; Lee, J. J.; Lötvall, J. O. Exosome-Mediated Transfer of MRNAs and MicroRNAs Is a Novel Mechanism of Genetic Exchange between Cells. *Nat. Cell Biol.* **2007**, *9* (6), 654−659.
(2) Tan, X.; Day, K. C.; Li, X.; Broses, L. J.; Xue, W.; Wu, W.; Wang, W. Y.; Lo, T.-W.; Purcell, E.; Wang, S.; Sun, Y.-L.; Khaing Oo, M. K.; Baker, B. M.; Nagrath, S.; Day, M. L.; Fan, X. Quantification and Immunoprofiling of Bladder Cancer Cell-Derived Extracellular Vesicles with Microfluidic Chemiluminescent ELISA. *Biosens. Bioelectron.: X* **2021**, *8*, 100066.
(3) Tian, T.; Zhu, Y.-L.; Zhou, Y.-Y.; Liang, G.-F.; Wang, Y.-Y.; Hu, F.-H.; Xiao, Z.-D. Exosome Uptake through Clathrin-Mediated Endocytosis and Macropinocytosis and Mediating MiR-21 Delivery. *J. Biol. Chem.* **2014**, *289* (32), 22258−22267.
(4) Fernando, M. R.; Jiang, C.; Krzyzanowski, G. D.; Ryan, W. L. New Evidence That a Large Proportion of Human Blood Plasma Cell-Free DNA Is Localized in Exosomes. *PLoS One* **2017**, *12* (8), No. e0183915.
(5) He, F.; Ye, Z.-Y.; Zhao, L.-D.; Yin, B.-C.; Ye, B.-C. Probing Exosome Internalization Pathways through Confocal Microscopy Imaging. *Chem. Commun.* **2019**, *55* (93), 14015−14018.
(6) Zheng, Z.; Li, Z.; Xu, C.; Guo, B.; Guo, P. Folate-Displaying Exosome Mediated Cytosolic Delivery of SiRNA Avoiding Endosome Trapping. *J. Controlled Release* **2019**, *311*−*312*, 43−49.
(7) Kato, K.; Kobayashi, M.; Hanamura, N.; Akagi, T.; Kosaka, N.; Ochiya, T.; Ichiki, T. Electrokinetic Evaluation of Individual Exosomes by On-Chip Microcapillary Electrophoresis with Laser Dark-Field Microscopy. *Jpn. J. Appl. Phys.* **2013**, *52* (6S), 06GK10.
(8) Im, H.; Shao, H.; Park, Y. I.; Peterson, V. M.; Castro, C. M.; Weissleder, R.; Lee, H. Label-Free Detection and Molecular Profiling of Exosomes with a Nano-Plasmonic Sensor. *Nat. Biotechnol.* **2014**, *32* (5), 490−495.
(9) Yang, Y.; Shen, G.; Wang, H.; Li, H.; Zhang, T.; Tao, N.; Ding, X.; Yu, H. Interferometric Plasmonic Imaging and Detection of Single Exosomes. *Proc. Natl. Acad. Sci. U. S. A.* **2018**, *115* (41), 10275−10280.
(10) Li, N.; Huang, Z.; Zhang, X.; Song, X.; Xiao, Y. Reflecting Size Differences of Exosomes by Using the Combination of Membrane-Targeting Viscosity Probe and Fluorescence Lifetime Imaging Microscopy. *Anal. Chem.* **2019**, *91* (23), 15308−15316.
(11) Chen, C.; Zong, S.; Wang, Z.; Lu, J.; Zhu, D.; Zhang, Y.; Cui, Y. Imaging and Intracellular Tracking of Cancer-Derived Exosomes Using Single-Molecule Localization-Based Super-Resolution Microscope. *ACS Appl. Mater. Interfaces* **2016**, *8* (39), 25825−25833.
(12) Qiu, G.; Gai, Z.; Tao, Y.; Schmitt, J.; Kullak-Ublick, G. A.; Wang, J. Dual-Functional Plasmonic Photothermal Biosensors for Highly Accurate Severe Acute Respiratory Syndrome Coronavirus 2 Detection. *ACS Nano* **2020**, *14* (5), 5268−5277.
(13) Tabakman, S. M.; Lau, L.; Robinson, J. T.; Price, J.; Sherlock, S. P.; Wang, H.; Zhang, B.; Chen, Z.; Tangsombatvisit, S.; Jarrell, J. A.; et al. Plasmonic Substrates for Multiplexed Protein Microarrays with Femtomolar Sensitivity and Broad Dynamic Range. *Nat. Commun.* **2011**, *2* (1), 466.
(14) Xu, W.; Wang, L.; Zhang, R.; Sun, X.; Huang, L.; Su, H.; Wei, X.; Chen, C.-C.; Lou, J.; Dai, H.; et al. Diagnosis and Prognosis of Myocardial Infarction on a Plasmonic Chip. *Nat. Commun.* **2020**, *11* (1), 1654.
(15) Lee, H.; Berk, J.; Webster, A.; Kim, D.; Foreman, M. R. Label-Free Detection of Single Nanoparticles with Disordered Nanoisland Surface Plasmon Sensor. *Nanotechnology* **2022**, *33* (16), 165502.
(16) Lee, H.; Lei, M.; Zhao, J.; Chen, G.; Hu, J.; Burns, Z.; Tian, F.; Liu, Z. Super-Resolution Raman Scattering Imaging Enabled by Rough Metal Films. *Nano Lett.* **2025**, *25* (22), 8954−8960.
(17) Lee, W.; Kang, B.-H.; Yang, H.; Park, M.; Kwak, J. H.; Chung, T.; Jeong, Y.; Kim, B. K.; Jeong, K.-H. Spread Spectrum SERS Allows Label-Free Detection of Attomolar Neurotransmitters. *Nat. Commun.* **2021**, *12* (1), 159.
(18) Cong, S.; Wang, Z.; Gong, W.; Chen, Z.; Lu, W.; Lombardi, J. R.; Zhao, Z. Electrochromic Semiconductors as Colorimetric SERS Substrates with High Reproducibility and Renewability. *Nat. Commun.* **2019**, *10* (1), 678.
(19) Yoo, H.; Lee, H.; Rhee, W. J.; Moon, G.; Lee, C.; Lee, S. A.; Shin, J.-S.; Kim, D. Disordered Nanocomposite Islands for Nanospeckle Illumination Microscopy in Wide-Field Super-Resolution Imaging. *Adv. Opt. Mater.* **2021**, *9* (15), 2100211.
(20) Chen, S.; Svedendahl, M.; Van Duyne, R. P.; Käll, M. Plasmon-Enhanced Colorimetric ELISA with Single Molecule Sensitivity. *Nano Lett.* **2011**, *11* (4), 1826−1830.
(21) Kedem, O.; Tesler, A. B.; Vaskevich, A.; Rubinstein, I. Sensitivity and Optimization of Localized Surface Plasmon Resonance Transducers. *ACS Nano* **2011**, *5* (2), 748−760.
(22) Szunerits, S.; Boukherroub, R. Sensing Using Localised Surface Plasmon Resonance Sensors. *Chem. Commun.* **2012**, *48* (72), 8999.
(23) Liu, L.; Huh, J. R.; Shah, K. Microbiota and the Gut-Brain-Axis: Implications for New Therapeutic Design in the CNS. *EBioMedicine* **2022**, *77*, 103908.
(24) Kim, R.; Sung, J. H. Recent Advances in Gut- and Gut−Organ-Axis-on-a-Chip Models. *Adv. Healthcare Mater.* **2024**, *13* (21), No. e2302777.
(25) Leung, C. M.; de Haan, P.; Ronaldson-Bouchard, K.; Kim, G.-A.; Ko, J.; Rho, H. S.; Chen, Z.; Habibovic, P.; Jeon, N. L.; Takayama, S.; et al. A Guide to the Organ-on-a-Chip. *Nat. Rev. Methods Primers* **2022**, *2* (1), 33.

(26) Kim, N. Y.; Lee, H. Y.; Choi, Y. Y.; Mo, S. J.; Jeon, S.; Ha, J. H.; Park, S. D.; Shim, J.-J.; Lee, J.; Chung, B. G. Effect of Gut Microbiota-Derived Metabolites and Extracellular Vesicles on Neurodegenerative Disease in a Gut-Brain Axis Chip. *Nano Convergence* **2024**, *11* (1), 7.
(27) Kim, M.-H.; Kim, D.; Sung, J. H. A Gut-Brain Axis-on-a-Chip for Studying Transport across Epithelial and Endothelial Barriers. *J. Of Ind. Eng. Chem.* **2021**, *101*, 126−134.
(28) Altug, H.; Oh, S.-H.; Maier, S. A.; Homola, J. Advances and Applications of Nanophotonic Biosensors. *Nat. Nanotechnol.* **2022**, *17* (1), 5−16.
(29) Lou, C.; Yang, H.; Hou, Y.; Huang, H.; Qiu, J.; Wang, C.; Sang, Y.; Liu, H.; Han, L. Microfluidic Platforms for Real-Time In Situ Monitoring of Biomarkers for Cellular Processes. *Adv. Mater.* **2024**, *36* (6), 2307051.
(30) Bezryadina, A.; Zhao, J.; Xia, Y.; Zhang, X.; Liu, Z. High Spatiotemporal Resolution Imaging with Localized Plasmonic Structured Illumination Microscopy. *ACS Nano* **2018**, *12* (8), 8248−8254.
(31) Lee, H.; Yoo, H.; Moon, G.; Toh, K.-A.; Mochizuki, K.; Fujita, K.; Kim, D. Super-Resolved Raman Microscopy Using Random Structured Light Illumination: Concept and Feasibility. *J. Chem. Phys.* **2021**, *155* (14), 144202.
(32) Son, T.; Moon, G.; Lee, H.; Kim, D. Metallic 3D Random Nanocomposite Islands For Near-Field Spatial Light Switching. *Adv. Opt. Mater.* **2018**, *6* (10), 1701219.
(33) Groß, H.; Heil, H. S.; Ehrig, J.; Schwarz, F. W.; Hecht, B.; Diez, S. Parallel Mapping of Optical Near-Field Interactions by Molecular Motor-Driven Quantum Dots. *Nat. Nanotechnol.* **2018**, *13* (8), 691−695.
(34) Son, T.; Lee, D.; Lee, C.; Moon, G.; Ha, G. E.; Lee, H.; Kwak, H.; Cheong, E.; Kim, D. Superlocalized Three-Dimensional Live Imaging of Mitochondrial Dynamics in Neurons Using Plasmonic Nanohole Arrays. *ACS Nano* **2019**, *13* (3), 3063−3074.
(35) Mudry, E.; Belkebir, K.; Girard, J.; Savatier, J.; Le Moal, E.; Nicoletti, C.; Allain, M.; Sentenac, A. Structured Illumination Microscopy Using Unknown Speckle Patterns. *Nat. Photonics* **2012**, *6* (5), 312−315.
(36) Moon, G.; Son, T.; Yoo, H.; Lee, C.; Lee, H.; Im, S.; Kim, D. Defocused Imaging-Based Quantification of Plasmon-Induced Distortion of Single Emitter Emission. *Light: Sci. Appl.* **2023**, *12* (1), 221.
(37) Noble, J. M.; Roberts, L. M.; Vidavsky, N.; Chiou, A. E.; Fischbach, C.; Paszek, M. J.; Estroff, L. A.; Kourkoutis, L. F. Direct Comparison of Optical and Electron Microscopy Methods for Structural Characterization of Extracellular Vesicles. *J. Struct. Biol.* **2020**, *210* (1), 107474.
(38) Zabeo, D.; Cvjetkovic, A.; Lässer, C.; Schorb, M.; Lötvall, J.; Höög, J. L. Exosomes Purified from a Single Cell Type Have Diverse Morphology. *J. Extracell. Vesicles* **2017**, *6* (1), 1329476.
(39) Gupta, D.; Liang, X.; Pavlova, S.; Wiklander, O. P. B.; Corso, G.; Zhao, Y.; Saher, O.; Bost, J.; Zickler, A. M.; Piffko, A.; et al. Quantification of Extracellular Vesicles in Vitro and in Vivo Using Sensitive Bioluminescence Imaging. *J. Extracell. Vesicles* **2020**, *9* (1), 1800222.
(40) Hall, C.; Lueshen, E.; Mošat', A.; Linninger, A. A. Interspecies Scaling in Pharmacokinetics: A Novel Whole-Body Physiologically Based Modeling Framework to Discover Drug Biodistribution Mechanisms in Vivo. *J. Pharm. Sci.* **2012**, *101* (3), 1221−1241.
(41) Ray, L. A.; Heys, J. J. Fluid Flow and Mass Transport in Brain Tissue. *Fluids* **2019**, *4* (4), 196.
(42) Kojima, R.; Bojar, D.; Rizzi, G.; Hamri, G. C.-E.; El-Baba, M. D.; Saxena, P.; Ausländer, S.; Tan, K. R.; Fussenegger, M. Designer Exosomes Produced by Implanted Cells Intracerebrally Deliver Therapeutic Cargo for Parkinson's Disease Treatment. *Nat. Commun.* **2018**, *9* (1), 1305.
(43) Han, J.; Sul, J. H.; Lee, J.; Kim, E.; Kim, H. K.; Chae, M.; Lim, J.; Kim, J.; Kim, C.; Kim, J.-S.; et al. Engineered Exosomes with a Photoinducible Protein Delivery System Enable CRISPR-Cas−Based Epigenome Editing in Alzheimer's Disease. *Sci. Transl. Med.* **2024**, *16* (759), No. eadi4830.
(44) Colombo, M.; Raposo, G.; Théry, C. Biogenesis, Secretion, and Intercellular Interactions of Exosomes and Other Extracellular Vesicles. *Annu. Rev. Cell Dev. Biol.* **2014**, *30* (1), 255−89.
(45) Petersen, J. D.; Mekhedov, E.; Kaur, S.; Roberts, D. D.; Zimmerberg, J. Endothelial Cells Release Hybrid Extracellular Vesicles: Microvesicles that Secrete Exosomes. *Biophys. J.* **2022**, *121*, 293a.
(46) Tian, T.; Zhu, Y.; Hu, F.; Wang, Y.; Huang, N.; Xiao, Z. Dynamics of Exosome Internalization and Trafficking. *J. Cell. Physiol.* **2013**, *228* (7), 1487−1495.
(47) Inotsuka, R.; Uchimura, K.; Yamatsu, A.; Kim, M.; Katakura, Y. γ-Aminobutyric Acid (GABA) Activates Neuronal Cells by Inducing the Secretion of Exosomes from Intestinal Cells. *Food Funct.* **2020**, *11*, 9285−9290.
(48) Polanco, J. C.; Hand, G. R.; Briner, A.; Li, C.; Götz, J. Exosomes Induce Endolysosomal Permeabilization as a Gateway by which Exosomal Tau Seeds Escape into the Cytosol. *Acta Neuropathol.* **2021**, *141*, 235−256.
(49) Mathieu, M.; Martin-Jaular, L.; Lavieu, G.; Théry, C. Specificities of Secretion and Uptake of Exosomes and Other Extracellular Vesicles for Cell-to-Cell Communication. *Nat. Cell Biol.* **2019**, *21*, 9−17.
(50) Halipi, V.; Sasanian, N.; Feng, J.; Hu, J.; Lubart, Q.; Bernson, D.; van Leeuwen, D.; Ahmadpour, D.; Sparr, E.; Esbjörner, E. K. Extracellular Vesicles Slow Down Aβ(1−42) Aggregation by Interfering with the Amyloid Fibril Elongation Step. *ACS Chem. Neurosci.* **2024**, *15*, 944−954.
(51) Asai, H.; Ikezu, S.; Tsunoda, S.; Medalla, M.; Luebke, J.; Haydar, T.; Wolozin, B.; Butovsky, O.; Kügler, S.; Ikezu, T. Depletion of Microglia and Inhibition of Exosome Synthesis Halt Tau Propagation. *Nat. Neurosci.* **2015**, *18*, 1584−1593.
(52) Fiandaca, M. S.; Kapogiannis, D.; Mapstone, M.; Boxer, A.; Eitan, E.; Schwartz, J. B.; Abner, E. L.; Petersen, R. C.; Federoff, H. J.; Miller, B. L.; et al. Identification of Preclinical Alzheimer's Disease by a Profile of Pathogenic Proteins in Neurally Derived Blood Exosomes: A Case-Control Study. *Alzheimer's Dementia* **2015**, *11*, No. e600.1−e607.1.
(53) Lee, Y. U.; Posner, C.; Nie, Z.; Zhao, J.; Li, S.; Bopp, S. E.; Wisna, G. B. M.; Ha, J.; Song, C.; Zhang, J.; et al. Organic Hyperbolic Material Assisted Illumination Nanoscopy. *Adv. Sci.* **2021**, *8* (22), 2102230.
(54) Lei, M.; Zhao, J.; Zhou, J.; Lee, H.; Wu, Q.; Burns, Z.; Chen, G.; Liu, Z. Super Resolution Label-Free Dark-Field Microscopy by Deep Learning. *Nanoscale* **2024**, *16* (9), 4703−4709.
(55) Palik, E. D. *Handbook of Optical Constants of Solids*; Elsevier: New York, 1985.
(56) Kalluri, R.; LeBleu, V. S. The Biology, Function, and Biomedical Applications of Exosomes. *Science* **2020**, *367* (6478), No. eaau6977.
(57) Kojima, R.; Bojar, D.; Rizzi, G.; Hamri, G. C.-E.; El-Baba, M. D.; Saxena, P.; Ausländer, S.; Tan, K. R.; Fussenegger, M. Designer Exosomes Produced by Implanted Cells Intracerebrally Deliver Therapeutic Cargo for Parkinson's Disease Treatment. *Nat. Commun.* **2018**, *9* (1), 1305.
(58) Jurgielewicz, B. J.; Yao, Y.; Stice, S. L. Kinetics and Specificity of HEK293T Extracellular Vesicle Uptake Using Imaging Flow Cytometry. *Nanoscale Res. Lett.* **2020**, *15* (1), 170.

https://doi.org/10.1021/acsnano.5c09164
ACS Nano 2025, 19, 30349−30360